RESEARCH ARTICLE

Applied Polymer SCIENCE WILEY

Mechanical, thermal, tribological, and flammability properties of polybutylene terephthalate composites: Comparing the effects of synthetic wollastonite nanofibers, natural wollastonite, and graphene oxide

Jia Xin Chan[1] | Joon Fatt Wong[1] | Azman Hassan[1] | Norhayani Othman[1] | Jeefferie Abd Razak[2] | Umar Nirmal[3] | Shahrir Hashim[1] | Yern Chee Ching[4] | Muhamad Zaini Yunos[5] | Ridwan Yahaya[6] | T. M. Sampath U. Gunathilake[7]

[1]Faculty of Chemical and Energy Engineering, Universiti Teknologi Malaysia, Johor Bahru, Johor, Malaysia

[2]Fakulti Kejuruteraan Pembuatan, Universiti Teknikal Malaysia Melaka, Hang Tuah Jaya, Durian Tunggal, Melaka, Malaysia

[3]Center of Advanced Mechanical and Green Technology, Faculty of Engineering and Technology, Multimedia University, Bukit Beruang, Melaka, Malaysia

[4]Faculty of Engineering, Universiti Malaya, Lembah Pantai, Kuala Lumpur, Malaysia

[5]Faculty of Mechanical and Manufacturing Engineering, Universiti Tun Hussein Onn Malaysia, Parit Raja, Johor, Malaysia

[6]Science and Technology Research Institute for Defence (STRIDE), Ministry of Defence, Kajang, Selangor, Malaysia

[7]Department of Polymer Science, University of Sri Jayewardenepura, Nugegoda, Sri Lanka

Correspondence
Azman Hassan and Norhayani Othman, Faculty of Chemical and Energy Engineering, Universiti Teknologi Malaysia, 81310, Johor Bahru, Johor, Malaysia.
Email: azmanh@cheme.utm.my and norhayani@utm.my

Abstract

Polybutylene terephthalate (PBT) composites were prepared with 1.0 phr synthetic wollastonite nanofibers (SWN), natural wollastonite (NW) and graphene oxide (GO) to study the effect of different fillers on mechanical, thermal, tribological, and flammability properties. The properties of PBT composites are related to the size, structure, and interfacial adhesion of the fillers in PBT matrix. PBT/SWN demonstrated the highest tensile strength and Young's modulus (6% and 9% increment), followed by PBT/NW (1.3% and 7% increment) and PBT/GO (2% decrement and 4% increment). PBT/SWN gave the highest degradation temperature (409°C), followed by PBT/GO (404.7°C). The maximum enhancement in wear resistance (73%) by PBT/SWN and anti-friction performance (26%) by PBT/GO evinced the excellent load-bearing ability of SWN and the great lubricating effect of GO. PBT/NW had the lowest peak heat release rate, smoke, and carbon dioxide production rate. This study shows that PBT composites have great potential in different automotive applications.

KEYWORDS

flame retardance, friction and wear, mechanical properties, polymer-matrix composites, thermal properties

1 | INTRODUCTION

Polybutylene terephthalate (PBT) is widely used in automotive sector for car seat frames, bumpers, and gears due to its processing advantages and superior dimensional stability.[1,2] However, compared to the other engineering polymers that are commonly used for automotive applications, such as polyamide (PA) and polyoxymethylene (POM), PBT usually exhibit poor tensile properties, thermal stability, and tribological properties. Thus, enhancing the mechanical, thermal, tribological, and flammability properties is important for the safety and service life of the products made of PBT. Various microscale fillers,[3,4] nano-scale fillers,[5–7] and hybrid fillers[1,8] were incorporated into PBT matrix to improve its functional properties. It was found that the type, shape, and size of the fillers played a significant role in determining the mechanical, thermal, and tribological properties of polymer composites.[9–13] Different types of filler had significantly different interfacial interactions with the polymer matrix, which can significantly affect the properties of composites.[14] In another work, acicular-shape wollastonite was found better in improving mechanical properties, while irregular-shaped wollastonite gave better thermal properties to polypropylene (PP) composites.[10] The comparison between commercial and synthetic silica nanoparticles was previously reported.[7] Moreover, nano-scale filler was reported to induce better performance enhancement as compared to their microcounterparts.[12]

Wollastonite has attracted great interest due to its 1D needle structure, biocompatibility, and its ability in improving the functional properties of polymer composites.[15,16] Series of works by Deshmukh et al. reported the effect of wollastonite on the mechanical, thermal, and tribological properties of PBT composites. The incorporation of wollastonite marginally increased tensile strength[3,4] and drastically increased Young's modulus.[3] The enhancement in mechanical properties was correlated to the good interfacial interaction between the PBT matrix and wollastonite. However, the elongation at break and impact strength of PBT composites deteriorated. The incorporation of wollastonite also increased the glass transition temperature (T_g), crystallization temperature (T_c), degree of crystallinity (X_c), and thermal stability of PBT composites.[3,14] Addition of 5 wt% wollastonite into the PBT matrix documented an improvement in wear resistance.[4] These wollastonite used were natural wollastonite (NW) with a broader range of micron sizes distribution.

With the recent focus on nanotechnologies, nano-scale wollastonite has been incorporated into polymers to form polymer nanocomposites with enhanced functional properties.[17–19] Nano-scale wollastonite with tunable shapes and sizes can be obtained through chemical routes.[20] Luyt and coworkers synthesized wollastonite nanoparticles through a sol–gel reaction route.[18] The PP/wollastonite nanocomposites exhibited higher tensile strength, Young's modulus, T_g, and thermal stability but lower elongation at break and T_c. A more recent study synthesized wollastonite nanoneedles through hydrothermal reaction and used it as filler in ultrahigh molecular weight polyethylene (UHMWPE) matrix.[17] Mechanical properties, wear resistance and X_c increased after the addition of wollastonite nanoneedles. However, melting temperature (T_m) and friction coefficient (μ) remain unchanged.

Graphene oxide (GO) as one of the most commonly used carbon-based nanofillers in polymer nanocomposites, has a distinct 2D layered structure. Recently, GO is a popular lubricating material used to enhance the mechanical and tribological properties of tribomaterials.[21,22] As far as GO-based PBT nanocomposites were concerned, Bian et al. prepared PBT/microwave exfoliated graphite oxide nanosheets (MEGONS) nanocomposites with good thermal and mechanical properties. The reinforcing effect of MEGONS was found dominant below 2 wt%.[23] A recent work reported the mechanical and thermal properties enhancement of PBT after the incorporation of poly (ethylene glycol) methacrylate-functionalized GO.[24] Another study claimed that the barrier effect of GO promotes the formation of compact carbon layer and thus improved the flame retardancy of PBT after its simultaneous addition with intumescent flame retardant.[6] Despite the potential of GO as a solid lubricant and flame retardant, the effect of GO on tribological and flammability properties of PBT nanocomposites has not been reported.

Although various properties of the wollastonite- and GO-reinforced PBT composites had been examined, it is of essential importance to directly compare the effect of different types of nanofiller on the functional properties of the PBT nanocomposites. Moreover, the comparison between micro- and nano-scale wollastonite was not reported. NW and synthetic wollastonite nanofibers (SWN) have 1D structures with different sizes and geometric structures. Thus, in the present work, PBT filled with NW, SWN, and GO were investigated in the aspect of mechanical, thermal, tribological, and flammability properties. This work focuses on the comparative study between the fillers with different types, shapes, and sizes. The structure–property relationship was investigated. Fourier-transform infrared spectroscopy (FTIR), field emission scanning electron microscopy (FESEM) and energy dispersive X-ray spectroscopy (EDS) were used to study the structural and morphological characteristics of PBT composites. Mechanical properties were studied by

conducting tensile and impact test, whereas differential scanning calorimetry (DSC) and thermogravimetric analysis (TGA) determine the thermal properties. Sliding test was conducted on a tribometer with pin-on-disc (POD) configuration to evaluate tribological properties, whereas flammability properties were determined through cone calorimetry analysis.

2 | EXPERIMENT

2.1 | Materials

PBT (1100-211M) was purchased from Chang Chun Plastics Co., Ltd, China. Analytical grade calcium nitrate tetrahydrate ($Ca(NO_3)_2 \cdot 4H_2O$) and sodium meta-silicate-pentahydrate ($NaSiO_3 \cdot 5H_2O$) were procured from QREC (ASIA) Sdn. Bhd, while liquefied ethanol with 95% v/v analytical grade was obtained from Vchem Sdn. Bhd. Malaysia for SWN production. The 600 mesh NW powder was purchased from Liaoning Metals & Minerals Enterprise Co., Ltd. UGOX™ United GO powder with 99% purity, an average thickness of 0.8–2.0 nm and a lateral dimension of 5–10 μm was supplied by United Nanotech Innovations Private Limited. All materials were used as supplied without any purification steps.

2.2 | Synthesis of synthetic wollastonite nanofibers

A simple hydrothermal reaction, followed by the calcination process was used to synthesis SWN.[20] The synthesis method of SWN was conducted according to our previous study with the reaction conditions of 80% (v/v) water to 20% (v/v) ethanol composition as the reaction medium, which heated at 200°C reaction temperature for 24 h hydrothermal reaction time.[20]

2.3 | Preparation of PBT and its composites

Prior to the compounding process, PBT resin and the filler powder (NW, SWN, and GO) were dried at 80°C for 24 h to remove the moisture. To achieve better filler dispersion, a two-stage melt blending approach was adopted. First, a master batch containing a higher amount of filler was compounded. Then, plain PBT was further incorporated into the masterbatch to fabricate PBT composites with NW, SWN, and GO, at 1.0 phr filler content. This 1.0 phr filler content was identified as the optimum filler content for PBT/SWN nanocomposites from our previous work.[25]

Single screw extruder (model: HAAKE Rheomex OS Thermo Scientific, USA) with 230 °C to 260°C barrel temperature profile and 60 rpm screw rotation speed was used for the melt blending. The extrudates were pelletized. The pellets were dried at 80°C for 24 h before the fabrication of test samples. Standard test specimen for tensile and impact test was fabricated using an injection molding machine (model: BOY XS, Germany). An injection pressure of 14 MPa and an injection speed of 100 mm/s were used for the filling process. While for plasticizing process, the barrel and nozzle temperature, pressure, and screw rotational speed were respectively set at 240 °C, 1 MPa and 170 rpm. Melted material was injected into the mold at 12 MPa holding pressure. Test specimens for tribological and cone calorimetry test were prepared using a compression molding machine (model: Guthrie, Malaysia) at 240°C and 30 MPa. Specimens were placed in a desiccator for at least 24 h before characterizations.

2.4 | Characterizations

2.4.1 | Fourier-transform infrared spectroscopy

FTIR spectrometer (model: Nicolet iS10 Thermo Scientific, USA) was used to obtain the FTIR spectra over the wavenumber range of 400–4000 cm^{-1}. The samples were prepared by mixing with KBr pellets, then pressed into thin sheets.

2.4.2 | Mechanical test

Tensile test and notched Izod impact test were performed. The average value of at least five samples was taken. Tensile test was performed on the standard dumbbell-shaped specimens according to ASTM D638 (Type IV) using a universal testing machine (model: AGS-J Shimadzu, Japan) at a crosshead speed of 10 mm/min and with 5 kN load cell. Notched Izod impact test was conducted on 12.5 mm × 63.0 mm × 3.2 mm test samples. The test was conducted using 11 Joule impact testing machine (model: HIT25P Zwick/Roell, Germany), according to ASTM D256 standard.

2.4.3 | Morphological characterization

The morphology of the fillers (NW, SWN, and GO) and the impact-fractured surface of PBT and its composites were observed using FESEM and EDS (model: SU8020 Hitachi, Japan) at an accelerating voltage of 5 kV. Prior

to the observation, the filler powders and fractured impact specimens were coated with a gold layer (i.e., purity of 99%) and mounted on carbon tape.

2.4.4 | Differential scanning calorimetry

The melting and crystallization behavior of PBT and its composites were determined by a DSC (model: DSC 1 Mettler Toledo, Switzerland). About 5–10 mg samples were sealed in aluminum pans and subjected to heating and cooling under nitrogen atmosphere at the rate of 10°C/min. The samples were heated from 30°C to 280°C and isothermally kept at 280°C for 5 min to erase their thermal history. Then, they were cooled to 30°C. X_c was calculated using Equation (1), where the melting enthalpy (ΔH_m) is obtained from the analysis in J/g, the theoretical value of enthalpy for a 100% crystalline PBT ($\Delta H_m°$) is equal to 140 J/g and w_{PBT} is the mass fraction of PBT matrix in the polymer composites.[26]

$$X_c = \frac{\Delta H_m}{\Delta H_m°(w_{PBT})} \times 100 \tag{1}$$

2.4.5 | Thermogravimetric analysis

Thermal stability of PBT and its composites were investigated through TGA (model: TGA 4000 Perkin Elmer, USA). About 5–10 mg sample was heated from 30°C to 600°C with the heating rate of 10°C/min under nitrogen condition.

2.4.6 | Tribological test

Wear and frictional test were conducted using a 10 mm × 10 mm × 20 mm test specimen on a POD tribo test machine according to ASTM G99. The tribo test machine comprised of a load cell (model: MT1041-75 Mettler Toledo, Switzerland) to measure the frictional forces and a digital infrared temperature sensor (model: FT-H10 Keyence, Japan) to measure the interface temperature of the stainless steel counterface and the test specimen. Dry sliding tests were conducted at room temperature (25 ± 3°C) under an applied normal load of 55 N, sliding speed of 1.0 m/s and sliding distance of 2500 m. Prior to each test, the stainless-steel counterface (AISI-304, 1250 HB) and the specimens were polished using silica carbide abrasive paper, grit no. 1000 to ensure proper intimate contact. The polished surfaces were cleaned with filtered compressed air, then wiped with a dry and clean cloth. A ±0.10 mg weight balance (model:

AW120 Shimadzu, Japan) was used to measure the weight loss of specimens. Sliding tests were repeated at least three times to obtain their average results. Specific wear rate (W_s) was determined using Equation (2), where W_s is in mm^3/N m, ΔV = volume difference (mm^3), F_N = applied normal load (N) and D = sliding distance (m). Friction coefficient (μ) was calculated using Equation (3). The morphologies of worn surfaces were analyzed using a metallurgical microscope (model: MT 7100 Meiji Techno, Japan).

$$W_s = \frac{\Delta V}{F_N D} \tag{2}$$

$$\mu = \frac{\text{Frictional force}}{\text{Normal applied force}} \tag{3}$$

2.4.7 | Cone calorimetry

Cone calorimeter (model: FESTEC International, Korea) was used to investigate the flammability properties of PBT and its composites under forced-flaming conditions, according to ISO 5660. The data obtained include time to ignition (TTI), peak of heat release rate (PHRR), time to PHRR, fire performance index (FPI), fire growth rate (FIGRA), peak of smoke release rate (PSPR), peak of carbon dioxide production (PCO$_2$P) and carbon monoxide production (PCOP). FPI is defined as the TTI/PHRR ratio, while FIGRA is the PHRR/time-to-PHRR ratio. The 100 mm × 100 mm × 3 mm test samples were wrapped on the side and bottom with aluminum foil, placed horizontally on the sample holder, then subjected to spark ignition and irradiated with 35 kW/m^2 external heat flux.[27]

3 | RESULTS AND DISCUSSION

3.1 | Structural characterizations of PBT and its composites

Figure 1a,b illustrates the FTIR spectra of NW, SWN, and GO in the range of 400–2000 and 2000–4000 cm^{-1}, respectively. In Figure 1, the characteristic peaks of SWN were labeled with the long dotted line to facilitate the comparison with the NW spectrum. The characterizing peaks of SWN at 452 and 473 cm^{-1} merged to become a broader and lower intensity band centered at 511 cm^{-1} in the NW spectrum. Moreover, NW exhibited a very broad band with two peaks centered at 881 and 1009 cm^{-1}, indicating the merging of distinct peaks of SWN at 904, 934, 973, 1030, and 1085 cm^{-1}. These bands
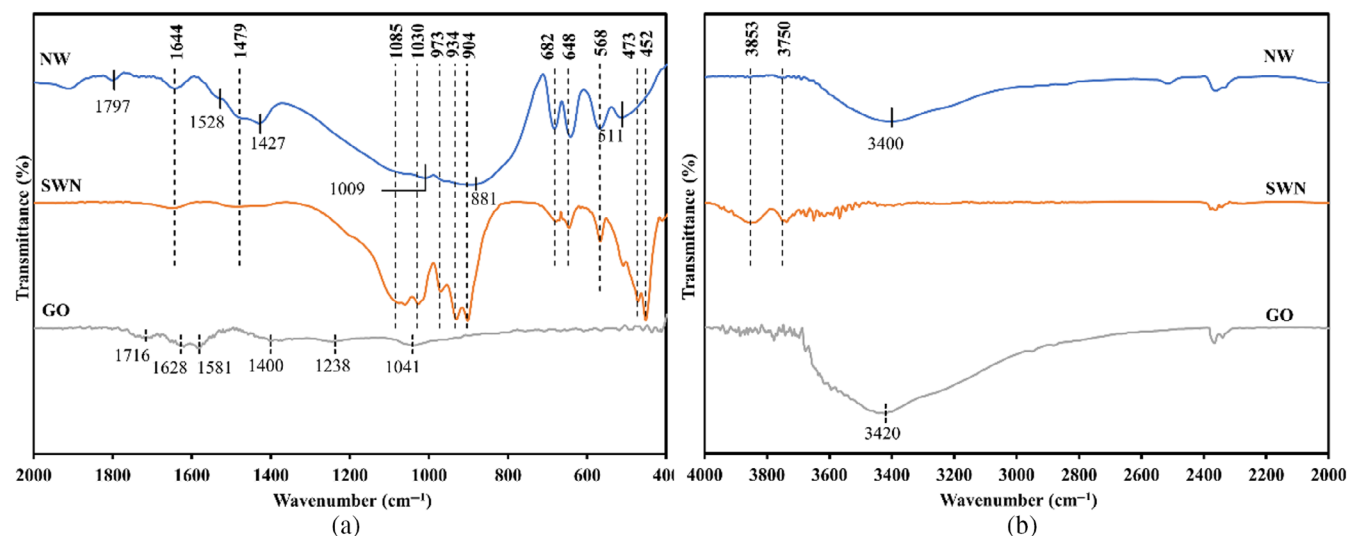
FIGURE 1 FTIR spectra of NW, SWN, and GO at wavenumber (a) 2000–400 cm^{-1} and (b) 4000–2000 cm^{-1}. [Color figure can be viewed at wileyonlinelibrary.com]
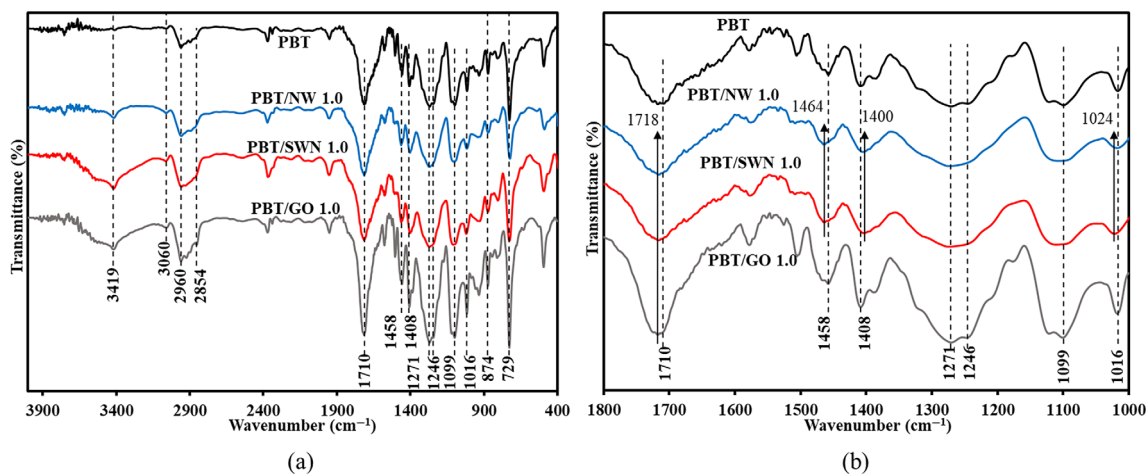

FIGURE 2 FTIR spectra of PBT, PBT/NW composite, PBT/SWN and PBT/GO nanocomposites at wavenumber (a) 4000–400 cm^{-1} and (b) 1800–1000 cm^{-1}. [Color figure can be viewed at wileyonlinelibrary.com]

in SWN feature the silicate chains in wollastonite.[28] Differences observed in the NW spectrum are probably due to the different Ca-to-Si ratios in NW as compared to SWN.[29] Another plausible reason is the structural disorder of crystal.[28,30] Besides, the appearance of a new peak at 1797 cm^{-1} can be attributed to the characteristic band of Ca(OH)$_2$.[29] The broad band centered at 3400 cm^{-1} is inferred as O—H stretching of hydroxyl group or water molecule absorbed in the sample.[28,30]

As shown in Figure 1, the characteristic bands of GO appear at 1716 cm^{-1} (stretching band of C═O in carboxyl and carbonyl group), 1628 and 1581 cm^{-1} representing C═C stretching vibration attributed to the unoxidized graphitic domain, 1400 cm^{-1} denoted to C—H bending vibration, 1238 and 1041 cm^{-1} corresponds to C—O stretching vibrations. Also, a strong broad band centered

at 3420 cm^{-1} was observed. This broad band at 2800–3700 cm^{-1} is identified as the stretching vibration of hydroxyl groups present in GO nanosheets. This evinces that the GO nanosheet had hydrophilic nature ascribed to the presence of oxygenated functional groups, including hydroxyl, epoxide, carboxyl, and carbonyl groups.[31]

The interaction between PBT matrix and the different fillers was also examined by FTIR analysis, as shown in Figure 2. Bands corresponding to PBT are seen in all composites. The presence of hydrogen bonding between SWN and PBT matrix can be inferred by the simultaneous appearance of broad peak centered at 3419 cm^{-1} and diminished peaks at 3500–3900 cm^{-1}, as well as the shifting of peaks in wavenumber ranging 1000–1800 cm^{-1}.[14] The shifting of peaks can also be observed in PBT/NW composite spectrum at the similar wavenumbers.
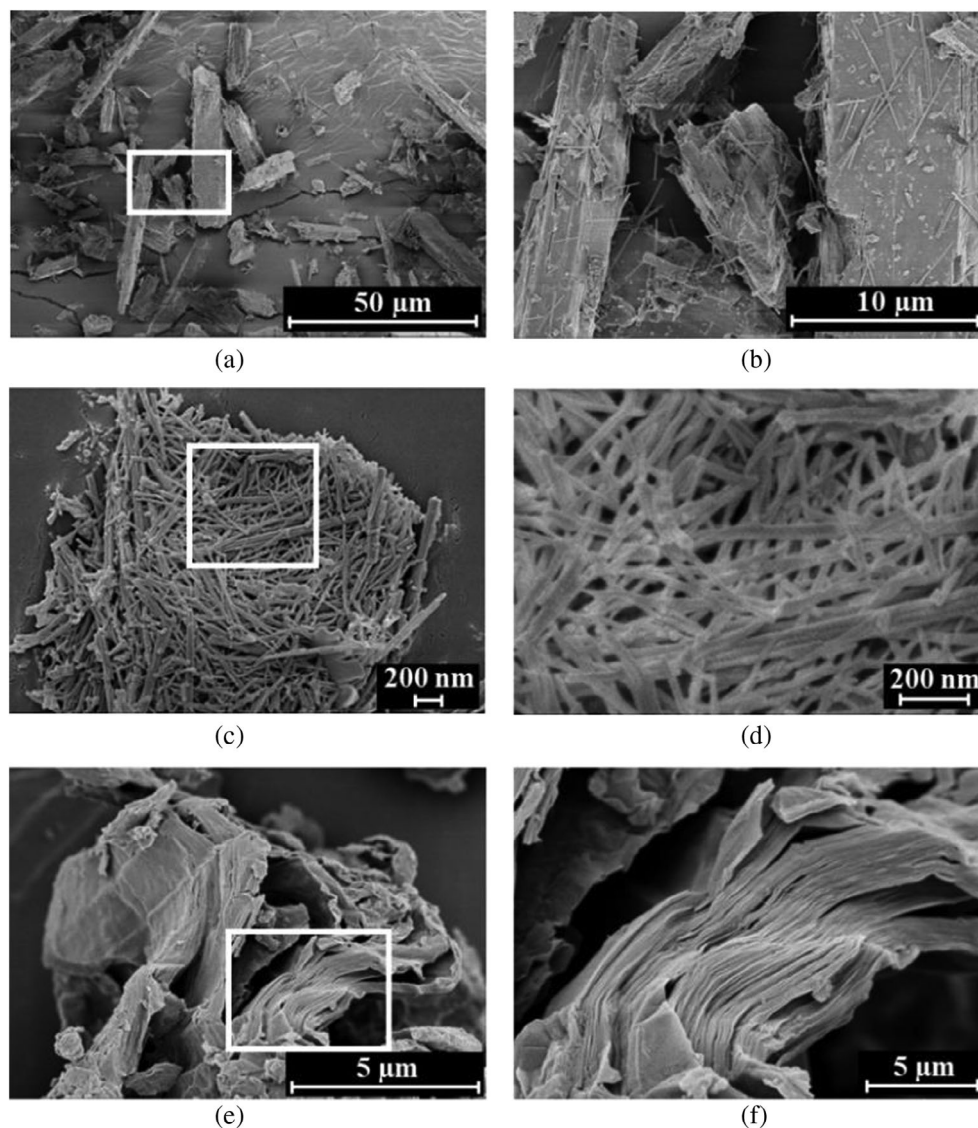
FIGURE 3 FESEM micrographs of (a) NW, (b) magnified NW at the white box area, (c) SWN, (d) magnified SWN at the white box area, (e) GO and (f) magnified GO at the white box area.

However, the weak band centered at 3419 cm^{-1} indicated that the interaction between NW and PBT was weaker than that of PBT/SWN nanocomposite. PBT/GO nanocomposite exhibited a broad band at around 3420 cm^{-1}, indicating the typical band of GO as shown in Figure 1b. This newly appeared broad band when compared to the spectrum of neat PBT was simply the superposition of the spectra of GO and PBT. Apart from this, no new band or shifting of band was observed, indicating that no interaction has taken place between GO and PBT matrix. Previous work also reported the absence of interaction between GO (1–5 wt%) and PET/PBT blend.[5]

3.2 | Morphological study on the fillers, PBT, and its composites

FESEM images in Figure 3 showed the distinct morphologies of the studied filler materials. Figure 3a showed

that the size and shape of NW were not uniform. Despite the presence of irregular particles, most of the NW particles portrayed 1D structure. A higher magnification micrograph in Figure 3b showed that there are many thin and long fiber-like or small irregular particles present on the surface of those large NW particles. Moreover, Figure 3c,d illustrated SWN as distinct fiber morphology. Unlike NW, SWN showed minimum grain shape particles. Figure 3d exhibited that the surfaces of SWN are smooth. Figure 3e,f showed that the bulk GO is in 2D structure with the folded or wrinkled phenomenon. GO nanosheets are physically bonded to each other by weak van der Waals forces and stacked regularly to form a micro-size bulk particle with many layers.[5,6] It is obvious that nano-size fillers (SWN and GO) tend to agglomerate due to their large specific surface area and high surface energy.[32]

To characterize the dispersion state of fillers in PBT matrix, the fracture surfaces of the composites were

FIGURE 4 FESEM images and EDS element mapping micrographs of the fracture surface of (a) PBT/NW 1.0 composite, (b) PBT/SWN 1.0 nanocomposite, and (c) PBT/GO 1.0 nanocomposite. [Color figure can be viewed at wileyonlinelibrary.com]
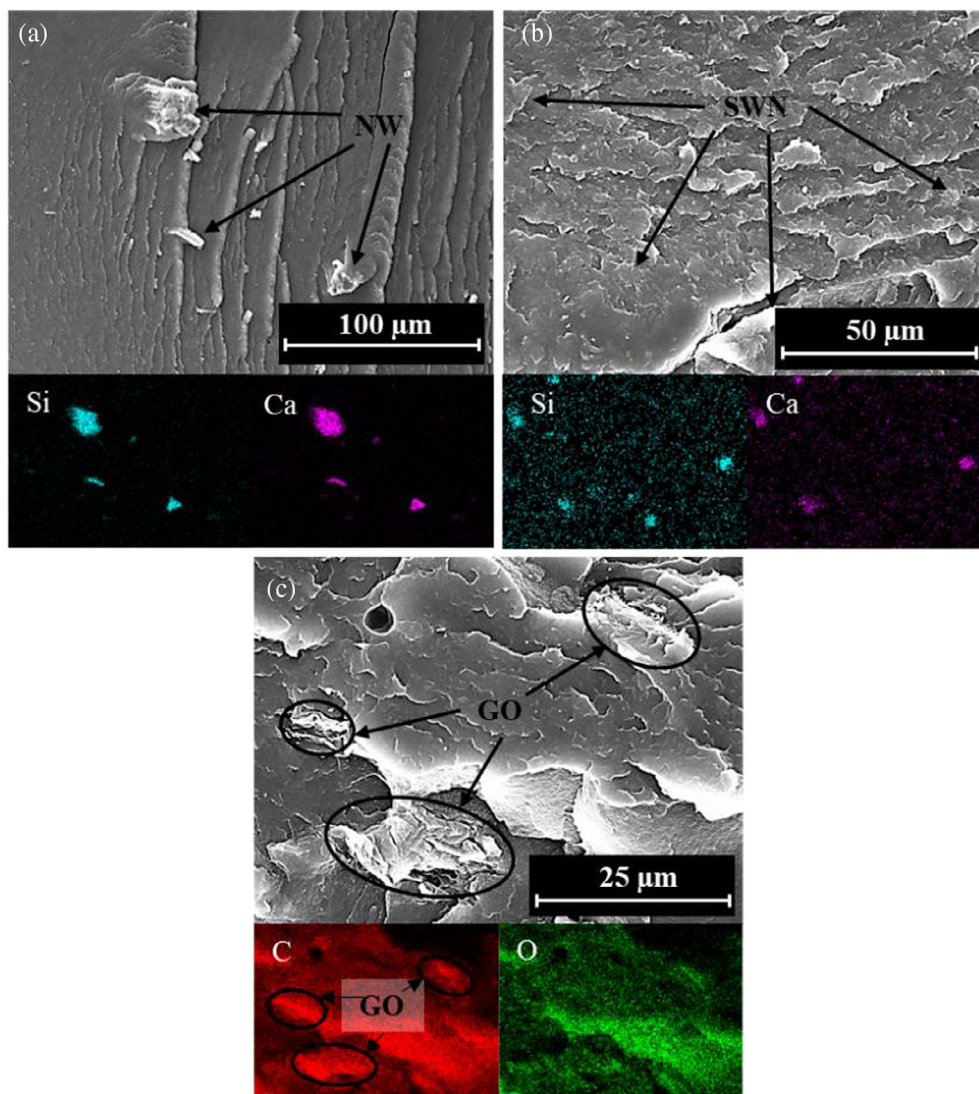
examined through FESEM and EDS analysis, as shown in Figure 4. The presence of SWN and NW were determined from EDS analysis and indicated by arrows in FESEM micrographs. The O, Si, and Ca elements confirmed the presence of wollastonite in the composite structure. Thus, the mapping analysis of Si (blue dots) and Ca (purple dots) were displayed to study the dispersion of NW and SWN. For both PBT/NW composite and PBT/SWN nanocomposite, detailed scans over the entire fractured surface in Figure 4a,b showed no obvious agglomerates. This is supported by the EDS elemental mapping which suggested well dispersion of SWN and NW. During the microscopic observations, agglomerated GO were clearly visible at the fractured surface, represented by Figure 4c. GO was not homogeneously dispersed in the PBT matrix. This is supported by the EDS analysis. GO was composed of C, H, and O elements.[6,23] C (red dots) and O (green dots) elements were used to indicate the presence of GO and were circled in Figure 4c. The presence of aggregates indicates

that the shear force generated during melt compounding is insufficient for the intercalation of PBT matrix into GO agglomerates. The shear force was not sufficient to diminish the van der Waals forces between GO nanosheets, also the functional groups present on the GO nanosheets were not readily interacting with the functional groups of PBT matrix. Thus, the dispersion of 2D filler is significantly more challenging than that of 1D filler.

The magnified FESEM micrographs are shown in Figure 5. Figure 5a revealed the exposure of NW particles on the fracture surface of PBT/NW 1.0 composite. It can be observed that part of the NW particle possessed rough surface, at which it was almost fully covered with PBT matrix. However, other parts of the particles demonstrated smooth surface with minimum attachment of matrix. The occurrence of small cavities around the NW particle, which are marked by the arrows, characterizes the relatively weak interfacial interactions between the filler and matrix. Figure 5b showed evidence of good
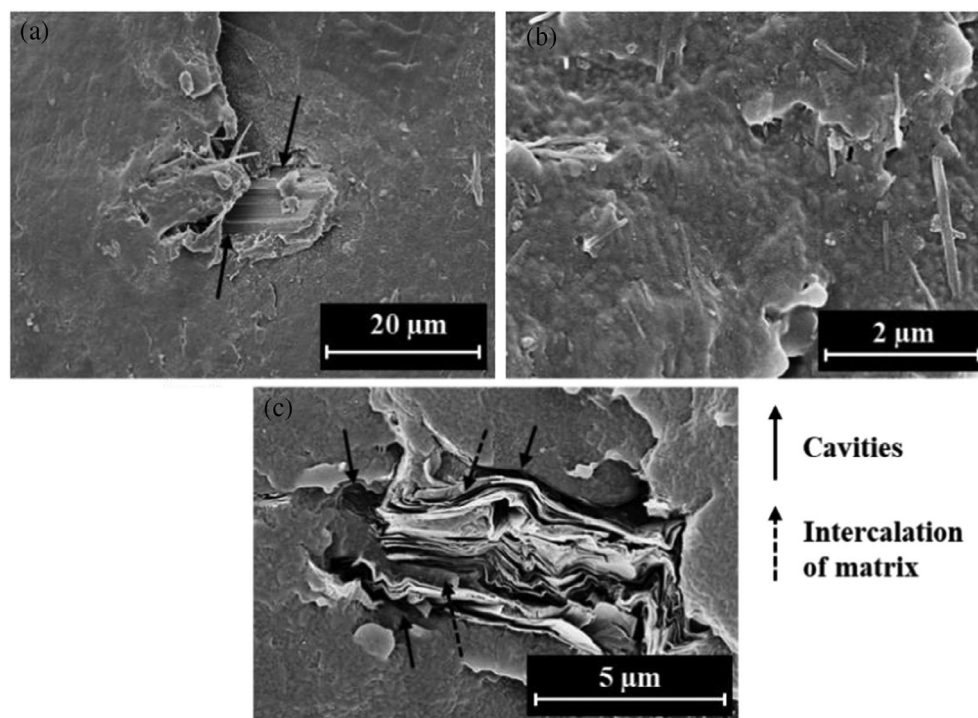
FIGURE 5 Magnified FESEM micrographs of (a) PBT/NW 1.0 composite, (b) PBT/SWN 1.0, and (c) PBT/GO 1.0 nanocomposite focused on the fillers.

interactions between the SWN and PBT matrix, in line with the FTIR result. Most of the SWN nanofillers appear embedded in the polymer matrix. It can be observed that some SWN or the tips of SWN were exposed at the fracture surface, and they possessed rough surfaces, covered with the matrix. The different observations for PBT/NW and PBT/SWN composites were due to their different size which significantly affected the total surface area per volume. In Figure 5c, it is seen that there is no interaction between GO agglomerates and the PBT matrix, evinced by the presence of cavities (marked by the arrows) at the filler-matrix interface and the smooth surface of the exposed GO agglomerates. The cavities formed between GO and PBT matrix not only hindered the stress transfer when stress was applied but also acted as the stress concentration points.[5,33] This increased the likelihood of GO being mechanically removed or detached from the matrix when stress was applied. The intercalation of matrix into GO agglomerates is limited (marked by dotted arrows). Microcracks surrounding the GO aggregates are noticeable. These observations can greatly affect the properties of PBT/GO 1.0 nanocomposite.

3.3 | Mechanical properties of PBT and its composites

Tensile stress–strain curves for PBT and PBT composites are presented in Figure S1. PBT and PBT/NW 1.0 composite exhibited ductile behavior, while PBT/SWN 1.0

and PBT/GO 1.0 nanocomposites were rather brittle. Stress–strain curve of pristine PBT was characterized by elastic deformation, yield point, localized necking, and strain hardening stage. The samples did not break over 200% strain. PBT/NW 1.0 composite displayed the same deformation behavior as PBT but fractured without showing strain hardening effect. However, it is obvious that the stress–strain curves changed from ductile to brittle behavior after the addition of SWN and GO. Both curves showed a fracture point shortly after the yield point. The observations on the stress–strain curve are consistent with the results reported in the literature. PP/1.5 vol% wollastonite nanocomposite exhibited slightly higher tensile strength and a significant drop in elongation at break as compared to the neat PP.[18] The incorporation of 5 wt% micro-wollastonite into PBT[3] and rPC/PC blend[34] slightly increased tensile strength but drastically reduced the elongation at break. Both tensile strength and elongation at break reduced after the addition of 1 wt% alkylated GO into PP matrix and 1 wt% GO into UHMWPE matrix.[35,36]

Figure 6a illustrated the average ultimate tensile strength of PBT and its composites. The highest tensile strength was demonstrated by PBT/SWN 1.0 nanocomposite, achieving 6% enhancement when compared to PBT. Tensile strength only increased by 1.3% for the PBT/NW 1.0 composite. Relative to their neat polymer matrix, polycarbonate (PC) and recycled-PC/PC composites reinforced with 5 wt% wollastonite also exhibited less than 3% increment in tensile strength.[34,37] However, the

FIGURE 6　Tensile properties include (a) tensile strength, (b) Young's modulus, (c) elongation at break, and (d) tensile toughness of PBT and its composites.
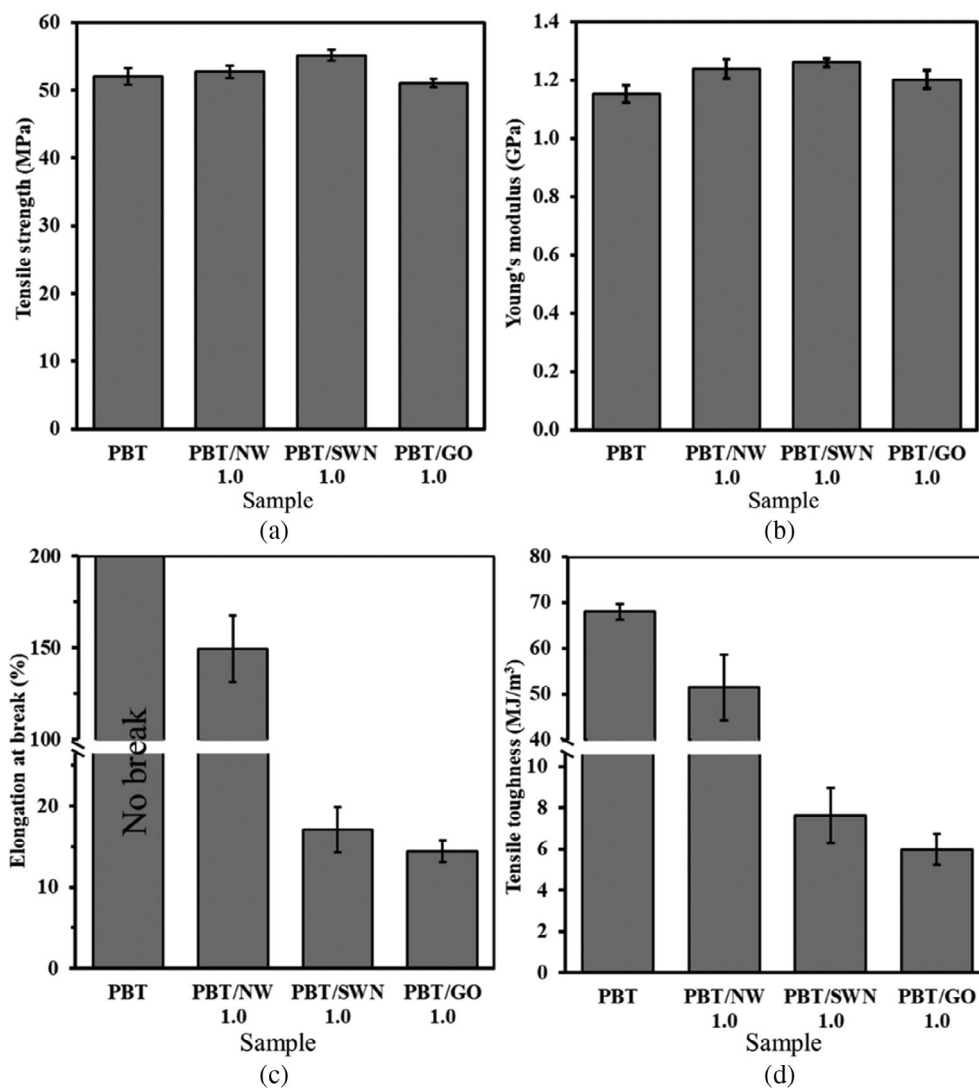
addition of GO lowered the tensile strength of PBT by 2%. This adverse effect of GO is negligible as compared to those observed in PP/alkylated GO[35] and UHMWPE/GO nanocomposites,[36] both at 1 wt%. However, this result is unexpected as GO played a good role in improving the tensile strength of most polymers, including PBT nanocomposites.[23,24,33] It is found that the tensile strength increased by about 16% at 1 wt% MEGONS addition in PBT matrix.[23] PBT/1 wt% GO nanocomposite showed about 18%[33] and 6%[24] higher tensile strength than their neat PBT, respectively.

Reinforcement is acquired by the transferring of applied stress from polymer matrix to the filler. Stress transfer is a function of filler size and shape, also the polymer-filler interfacial contact.[38,39] Filler with a smaller size, higher aspect ratio and better interfacial adhesion with the polymer matrix permitted better stress transfer between matrix and filler, then effectively increased the tensile strength.[38] The larger interfacial area attained by SWN as compared to NW induced better interaction with

the polymer matrix and facilitated stress transfer from the polymer matrix to rigid filler when stress was applied.[39] The slight decrement in tensile strength resulting from the incorporation of GO is attributed to its agglomeration, as well as its poor interactions with the PBT matrix.[5,24] This is supported by the FTIR and FESEM analysis. The mechanical mixing is insufficient in achieving a homogeneous dispersion of GO in PBT matrix. Besides, the presence of GO also diminished the continuity of polymer matrix, and thus limited the stress transfer at the filler/matrix boundary region.

Figure 6b,c, respectively, depict Young's modulus and elongation at break of PBT and its composites. Stiffness, indicated by Young's modulus, of the polymer composites can be improved by adding rigid and stiff filler into the polymer matrix. All reinforced PBT composites had higher Young's modulus than pure PBT. The presence of filler in PBT matrix, regardless of its size and shape, had restricted the polymer macromolecule chain from flowing past one another. The enhancement of about 7%, 9%,

and 4% in Young's modulus over neat PBT were obtained with the incorporation of NW, SWN, and GO fillers, respectively. SWN contributed a higher Young's modulus than NW as it restricted the mobility of polymer chains more effectively when pulling stress was applied. Due to the stacking of GO, it has limited hindering effect on polymer chains and exhibited the lowest stiffness among the composites.

Rigid NW, SWN, and GO exhibited low elongation properties and hindered the movement of polymer chains, thus eventually reducing the ductility of PBT composites. Tensile toughness shown in Figure 6d exhibited similar behavior as elongation at break in Figure 6c. The reinforced PBT composites demonstrated lower toughness compared to that of pristine PBT, indicating that they had less capability to absorb energy. Pure PBT did not break up to 200% strain and its tensile toughness was calculated as 68 MJ/m^3 at strain 200%. PBT/NW composite still maintained the ductile properties of PBT matrix, where the samples fractured at 149.6% strain. Whereas, both PBT/SWN and PBT/GO nanocomposites were brittle and fractured before reaching 20% elongation. Compared to PBT, the incorporation of NW, SWN, and GO nanofillers gave about 24%, 89%, and 91% toughness reduction, with the value of 51.4, 7.6, and 6.0 MJ/m^3. At the same filler loading, SWN possessed higher surface area when compared to NW. The stronger interfacial interactions restricted the plastic deformation of the polymer matrix around SWN nanofillers. Thus, PBT/SWN nanocomposite fractured at low elongation at break, without much plastic deformation and absorbed little energy. PBT/GO nanocomposite showed the lowest elongation at break and tensile toughness. It can be explained by the stress concentration effect of the staking GO.[23] The cavities formed between GO and PBT matrix have acted as the stress concentration sites.[33] GO nanofiller can be easily detached from the PBT matrix with minimum energy dissipation.

Like the results of elongation at break and tensile toughness, PBT composites had lower impact strength when compared to pristine PBT. Taking neat PBT as the benchmark in Figure 7, PBT/NW, PBT/SWN, and PBT/GO composites demonstrated 10.5%, 8.8%, and 14% reduction. respectively. In agreement with the previous work on planar-shape mica- and whisker-shape wollastonite-filled high-density polyethylene (HDPE) composites at filler loading of 5–15 wt%, GO with platelet shape gave lower impact strength as compared to PBT composites reinforced with acicular shape SWN and NW.[9] Owning to the poor interfacial interactions between filler and PBT matrix, micro-cavitation can easily form and build up stress, thus providing sites for crack initiation. After the crack is initiated, energy is mainly consumed through matrix deformation that led to fracture and filler pull-out. The poor interaction can be observed at the tips
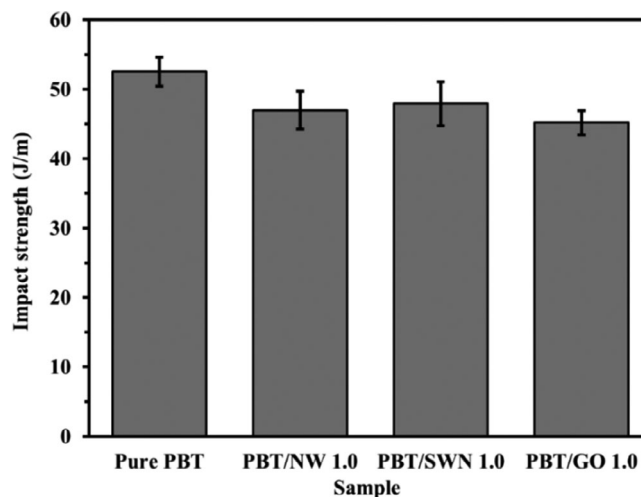

FIGURE 7 Notched Izod impact strength of PBT and its composites.

of the 1D-structured SWN and NW fillers, also the stacks of GO. PBT/SWN nanocomposite exhibited slightly higher impact strength when compared to PBT/NW composite due to the better interfacial interactions and higher total contact area of SWN, impeding the formation of cavitation. The agglomeration of GO nanosheets and its poor interfacial adhesion with PBT matrix promoted the pull-out of nanofillers during crack propagation, inducing very little plastic deformation of the surrounding polymer matrix.[33] Thus, PBT/GO nanocomposites exhibited the lowest impact strength of 45.2 J/m.

Stiff fillers can enhance Young's modulus of polymer, but it is detrimental to the impact strength. A significant increment in tensile strength and Young's modulus had been achieved by incorporating SWN. However, it must be noticed that the addition of NW gave adequate ductility to the PBT composite. From the standpoint of mechanical properties, GO nanofiller is only beneficial to Young's modulus of PBT nanocomposites. To identify the balance mechanical properties in terms of stiffness and toughness, a graph of Young's modulus versus impact strength was plotted in Figure 8. PBT has high impact strength but low Young's modulus. In contrast, PBT/GO nanocomposite demonstrated slightly higher modulus but the lowest impact strength properties. PBT/SWN nanocomposite showed the best combination with the highest Young's modulus and higher impact strength than other PBT composites.

3.4 | Melting and crystallizing behavior of PBT and its composites

Figure 9a showed the thermograms obtained from heating scan, while Figure 9b illustrated the cooling scan.
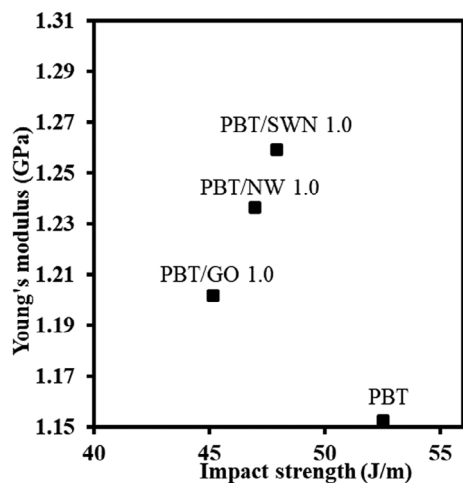
FIGURE 8 Overall mechanical properties of PBT and its composites in terms of stiffness and toughness.

The key calorimetric parameters were listed in Table 1. Neat PBT and its composites exhibited single melting peak in the heating scan. In the presence of fillers, T_m slightly shifted from ~224°C for neat PBT to ~225°C for PBT/NW 1.0 composite and PBT/GO 1.0 nanocomposite, 226.5 °C for PBT/SWN 1.0 nanocomposite. The T_m value of wollastonite-filled PBT with 5–30 wt% wollastonite content also varied in a narrow temperature range of 1.5°C.[3] About 1°C increment in T_m was observed when 1 wt% GO was incorporated in PBT.[33] The slight increment in T_m is in accordance with the slightly narrower melting peak width of composites than the peak of neat PBT. These indicate that the presence of NW, SWN, and GO slightly increased the crystal perfection of PBT in the composites.[10] NW, SWN, and GO gave insignificant raise in the ΔH_m value, which also corresponded to the insignificant increment in X_c value. This is due to the combined action of fillers in the polymer matrix, in terms of their nucleation effect and hindrance effect on the mobility of the polymeric chains upon crystallization.[40] T_c can be obtained from the exothermic peak temperature, shown in Figure 9b. The incorporation of fillers into PBT matrix elevated the T_c and onset crystallization temperature ($T_{c,o}$) by 2–4°C and 3–6°C, respectively. This implied that all the fillers had acted as heterogeneous nucleating agents to promote the crystallization of composites during the cooling scan.[10,40] Also, the enthalpy of crystallization (ΔH_c) values of PBT composites were higher than that of neat PBT, as the exothermic peaks of the composites were broader. The broadening of the peaks implies that these fillers acted as nucleating agents and barriers, at the same time, to the movement of polymer chains.[23]

3.5 | Thermal degradation behavior of PBT and its composites

The TGA analysis of pristine PBT and its different composites were showed in Figure S2 and Table 2. All samples showed similar single-step degradation curves. This indicates that the inclusion of fillers did not change the degradation mechanism of the PBT matrix. The main thermal degradation occurred between 350°C and 450°C. According to Table 2, the addition of fillers increased the degradation temperatures, such as onset and end set degradation temperature (T_{onset} and T_{endset}), degradation temperature at 20% mass loss (T_{20}), 50% mass loss (T_{50}) and maximum degradation rate (T_{max}). This suggests the higher thermal stability of PBT composites due to the thermal stability and physical barrier effect of the fillers, as well as their high heat conductivity and thermal diffusivity.[18,23,33] NW increased T_{onset} by 1.1°C and T_{max} by 4.3°C, while GO raised about 9–11°C for T_{onset} and T_{max}. The highest degradation temperatures were observed for PBT/SWN nanocomposite, showing 11.5°C and 13.8°C higher T_{onset} and T_{max} than neat PBT. Significant improvement in thermal degradation temperature (18°C) by 2.1 wt% nano-size wollastonite had been reported previously.[41] Incorporation of low-loading wollastonite (1–7 wt%) also gave slight improvement (1–3 °C) to poly(butylene adipate-co-terephthalate) composites.[42] Literature as well-reported great enhancement in degradation temperatures of PBT nanocomposite (10–15°C and 9–10°C) after the incorporation of 1.0 wt% GO and MEGONS, respectively.[23,33] In the perspective of residue weight, PBT/SWN nanocomposite produced the highest amount of char, followed by PBT/NW composite and PBT/GO nanocomposite. In fact, the incorporation of GO slightly reduced the char formation by 0.5 wt%. This is in agreement with the earlier work, where the addition of GO into PBT matrix did not show more char formation at the end of the TGA analysis.[33]

Compared to PBT/SWN nanocomposites, PBT/NW composites had inferior thermal stability. It is important to note that the higher surface area of SWN played a key role in this context.[11] SWN with larger surface area to volume ratio due to its nano size, possesses greater physical barrier effect. Also, the effect of its high thermal stability, heat conductivity and heat diffusivity is more obvious when the surface area is greater. PBT/GO nanocomposite degraded at temperatures slightly lower than PBT/SWN nanocomposite. This is attributed to the different dispersion states and thermal stability of SWN and GO. The stacking of GO in PBT matrix may limit the delay in degradation due to its limited barrier effect.[43] Besides, the poor interfacial interactions between GO and PBT matrix can lead to greater thermal boundary
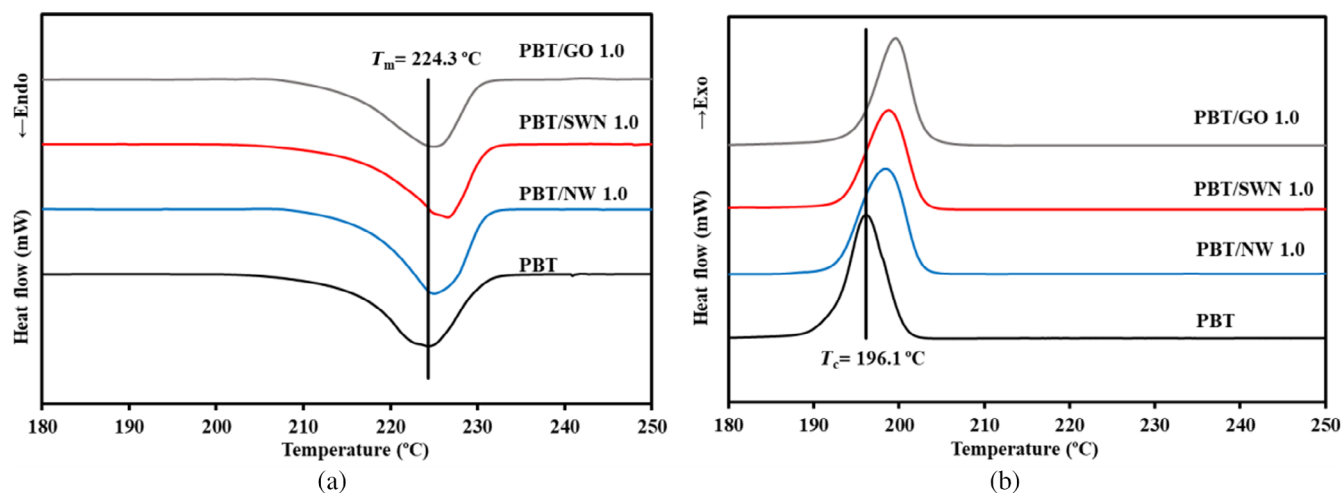
FIGURE 9 DSC thermograms of neat PBT and its composites with different types of filler obtained from (a) heating scan and (b) cooling scan. [Color figure can be viewed at wileyonlinelibrary.com]

TABLE 1 DSC parameters for neat PBT and its composites.

Sample	Heating			Cooling		
	T_m (°C)	ΔH_m (J/g)	X_c (%)	$T_{c,o}$ (°C)	T_c (°C)	ΔH_c (J/g)
PBT	224.3	49.3	35.2	203.4	196.1	49.3
PBT/NW 1.0	225.0	49.2	35.5	206.2	198.5	54.8
PBT/SWN 1.0	226.5	50.5	36.4	207.8	198.8	53.6
PBT/GO 1.0	224.8	49.2	35.5	209.8	199.7	54.8

TABLE 2 TGA results of PBT and its composites.

Sample	T_{onset} (°C)	T_{endset} (°C)	T_{20} (°C)	T_{50} (°C)	T_{max} (°C)	Residue weight at 600°C (wt%)
PBT	372.5	411.7	377.0	392.0	395.2	2.20
PBT/NW 1.0	373.6	415.2	381.8	396.9	399.5	3.89
PBT/SWN 1.0	384.0	423.0	393.0	406.0	409.0	3.92
PBT/GO 1.0	383.7	422.7	390.7	403.7	404.7	1.67

resistance and create hot spots in the nanocomposite. These local hot spots initiate the self-propagating reduction of GO, resulting in lower residue weight.[44]

3.6 | Tribological properties of PBT and its composites

Figure S3 demonstrated the curves of μ versus sliding distance. The curves of pure PBT and its composites can be divided into running-in period and steady state. At the running-in period, the μ value of all samples, except for PBT/GO 1.0 nanocomposite, increases first, then decreases, and at last stabilized at the steady stage. This is attributed to the small actual contact surface between tribomaterial and the counterface, also the occurrence of

plastic deformation.[45] PBT/GO nanocomposite had μ value increased with a lower gradient at the initial stage. Figure S4 showed the temperature profile and average interfacial temperature of PBT and its composites. The interface temperature increased almost linearly with sliding distance for all samples. Pristine PBT, its NW- and SWN-reinforced composites exhibit very close temperature variation up to the sliding distance of approximately 700 m. Whereas, PBT/GO had lower interface temperature up to the same distance. This might be the reason behind the different behavior of μ curve at the initial sliding period.[45] Severe plastic deformation at high interface temperature can result in a higher μ value. Thus, μ values of PBT, NW- and SWN-filled composites raised drastically at the running-in period, whereas PBT/GO nanocomposites showed a moderate increasing trend of μ.
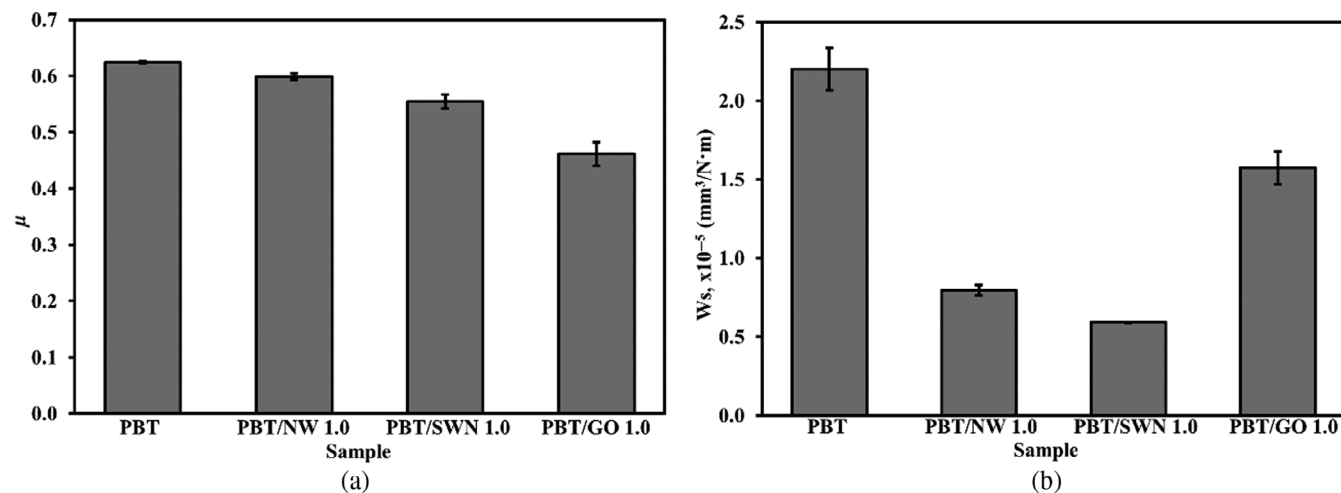
FIGURE 10 (a) Friction coefficient, μ and (b) specific wear rate, W_s of PBT and PBT composites (i.e., applied load: 55 N, velocity: 1.0 m/s, sliding distance: 2500 m).

Figure S4b evinced that the incorporation of fillers slightly lowered the average interface temperature at the steady-state period. The temperature of both PBT/NW composite and PBT/SWN nanocomposite decreased by approximately 3%, but that of PBT/GO nanocomposite was reduced by 0.4°C only.

The average μ and W_s of all the composites were revealed in Figure 10. Compared to pristine PBT, the incorporation of NW, SWN, and GO led to friction reduction and better wear resistance. The lubricating effect of fillers and the formation of transfer film at the sliding interface are plausible reasons behind the tribological properties enhancement.[22,46] Different fillers exhibited different tribological behaviors, owing to their different morphologies, structures, and interfacial interactions with the PBT matrix.[12] The incorporation of NW, SWN, and GO reduced μ from 0.624 for neat PBT to 0.599, 0.554, and 0.461 for PBT/NW 1.0 composite, PBT/SWN 1.0 and PBT/GO 1.0 nanocomposites, respectively. NW lowered the μ value by 4%, whereas SWN contributed to an 11% decrement. This can be explained by the surface morphologies of worn surfaces, found in the following paragraphs. Meanwhile, PBT/GO nanocomposite demonstrated the greatest friction reduction of 26%, owing to the structure and morphology of GO. The previous study documented the better lubricating ability of 2D structure filler than 1D structure filler.[46] GO induced about 50% lower μ than CNTs when they were incorporated into epoxy matrix at 1.25 wt%.[46] The lubricating ability of GO originates from its multilayer stacking structure.[21,22] The occurrence of interlayer sliding is accompanied by the lower shear resistance at the sliding surface.[32]

PBT/NW, PBT/SWN, and PBT/GO composites have W_s as low as 64%, 73%, and 28% than that of neat PBT,

respectively. Although W_s of the PBT/GO nanocomposite was lower than neat PBT, its wear resistance ability was poorer when compared to PBT/NW and PBT/SWN composites. This is attributed to the poor dispersion of GO and its poor interfacial interaction with the PBT matrix.[32,47] These averted the stress transfer between GO and PBT matrix at the sliding surface. With this, the load-bearing ability of PBT/GO nanocomposite was poor, and thus ease the surface damage during sliding. On the other hand, PBT/SWN nanocomposite and PBT/NW composite exhibited great improvement in wear resistance due to the reinforcement of wollastonite filler. Due to the larger contact area of SWN compared to NW, stress transfer at the sliding surface was promoted in PBT/SWN nanocomposite, and thus the greatest wear resistance was reported.[48] The anti-wear performance of the composites aligned with their mechanical strength. In other words, excellent tensile strength is beneficial to the wear resistance properties.

The worn surfaces of composites were investigated under an optical microscope, as shown in Figures 11 and S5 and S6. The worn surface of neat PBT (Figure 11a) revealed the ploughing scars directed parallel to the sliding direction and the uneven scuffing patches, which are associated with a combination of abrasion and adhesion wear mechanisms. The softened material on the worn surface made evident the involvement of plastic deformation. Consistent with its inferior μ and W_s, no back transfer film was found on the worn surface of PBT, rather large wear debris was observed in Figure S5a. PBT composites still underwent a combination of adhesive and abrasive wear mechanisms as shown in Figure 11. However, the adhesive wear was alleviated after the incorporation of fillers. Also, the worn surfaces of composites
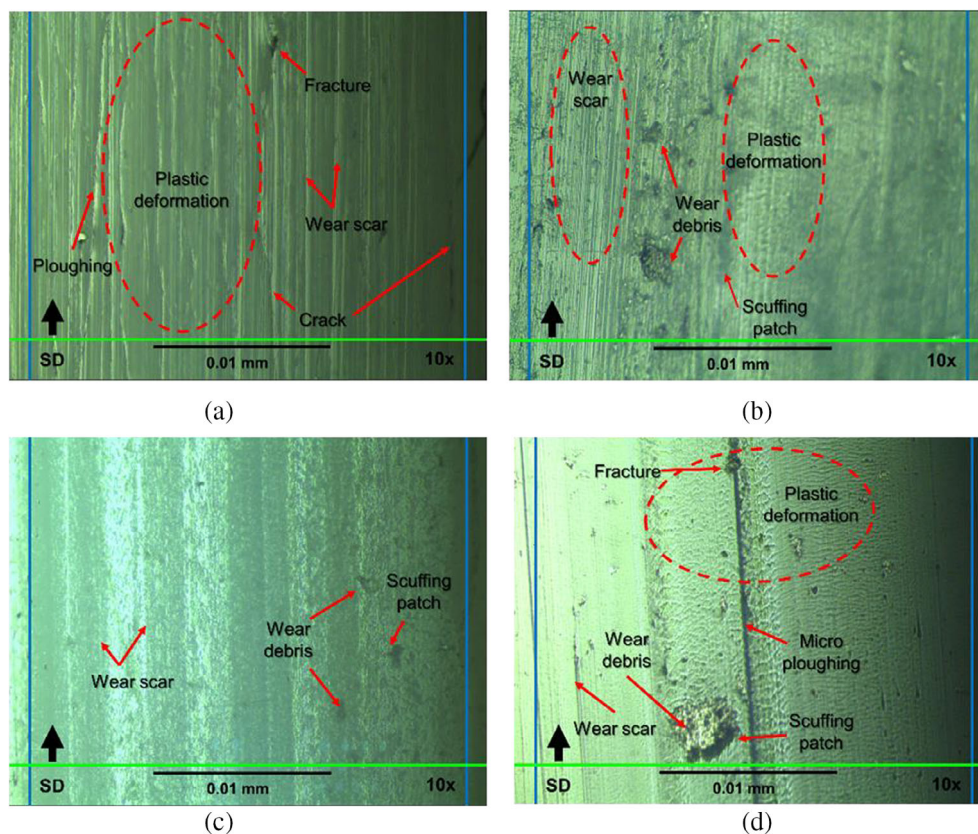
FIGURE 11 Optical microscopy images of the worn surfaces of (a) neat PBT, (b) PBT/NW 1.0 composite, (c) PBT/SWN 1.0 nanocomposite, and (d) PBT/GO 1.0 nanocomposite after sliding test under a load of 55 N and a sliding speed of 1.0 m/s. (remark: SD-sliding direction). [Color figure can be viewed at wileyonlinelibrary.com]

were much smoother when compared to that of neat PBT. The incorporation of fillers promoted the formation of back transfer film, which protects the pin from sliding against asperities of the metal counterface, then reduces the friction force.

Detailed microscopy images of the PBT/NW 1.0 composite revealed shallower plowing scars and alleviated plastic deformation occurring. Owning to the reinforcing ability of NW, the wear debris of PBT/NW composite was smaller in size than neat PBT and PBT/GO nanocomposite, but slightly bigger than the wear debris of PBT/SWN nanocomposite. Interestingly, a large amount of NW particles was found lying on the worn surface, as shown in Figure S7. This observation evinces the poor interfacial interaction between NW and PBT matrix and hence they were easily worn off from the composite. This detachment caused the loss of load-bearing capacity of PBT/NW composite at the sliding surface, leading to larger wear debris and higher W_s than PBT/SWN nanocomposite. Due to its high angularity, the detached NW particles may also cause abrasion on the worn surfaces during sliding.[49] Small back transfer film can be found on the worn surface of PBT/NW composite (Figure S6a). Both factors correspond to the highest μ value of PBT/NW 1.0 composite among the PBT composites.

The smoothest worn surface was observed for PBT/SWN 1.0 nanocomposite. The ploughing and wear scars on the worn surface are the shallowest among the sliding pins. This is attributed to the lower angularity of SWN as compared to NW and GO, which will not cause serious abrasion.[49] Plastic deformation phenomenon was also very much alleviated. Due to the better reinforcing ability of SWN, the size of the back transfer films observed for PBT/SWN nanocomposite were larger as compared to that of PBT/NW composite, whereas the wear debris formed was smaller. As the sliding test progressed, the debris merged and compacted under the load, eventually forming the transfer film at the sliding interface.[4] The larger back transfer film promoted a larger area of polymer-polymer sliding instead of direct polymer-metal sliding, and thus enhanced the tribological performance.

PBT/GO 1.0 nanocomposite exhibited the lowest μ but high W_s. It also revealed a combination of adhesive and abrasive wear mechanisms. However, microploughing scars were found on the worn surfaces, with deeper depth as compared to those worn scars of PBT/NW and PBT/SWN composite. Those abrasive scars are attributed to the agglomerated wear debris which could have acted as the third body at the sliding interface. This is evinced by the presence of large wear debris on the worn surface. The stacking of GO and its poor interactions with the PBT matrix can easily lead to large material removal, resulting in lower wear resistance.

TABLE 3 Key data of PBT and its composites from the cone calorimeter test.

Sample	TTI (s)	Time to PHRR (s)	PHRR (kW/m^2)	FIGRA (kW/ m^2.s)	FPI (m^2 s/kW)	PSPR (m^2/s)	PCO$_2$P (g/s)	PCOP (g/s)
PBT	53	162	572	3.5300	0.0927	0.1249	0.4672	0.0107
PBT/NW 1.0	44	155	474	3.0573	0.0929	0.1094	0.3779	0.0082
PBT/ SWN 1.0	50	155	495	3.1921	0.1011	0.1236	0.4024	0.0089
PBT/GO 1.0	42	147	509	3.4611	0.0826	0.1104	0.3907	0.0078

Although the ploughing scars on PBT/GO 1.0 nanocomposite's worn surface were deeper, its μ value remained low. This is attributed to the multilayer structure of GO, as well as the formation of large back transfer film, shown in Figure S6c. During the sliding test, the interlayer sliding of GO occurred and contributed a great lubricating effect to the sliding interface.[32,50]

3.7 | Flammability properties of PBT and its composites

The flammability results obtained from the cone calorimeter investigation are summarized in Table 3. All samples exhibited the typical heat release rate (HRR) curve of a thin sample as illustrated in Figure S8. With respect to neat PBT, the addition of NW, SWN, and GO led to a reduction in PHRR of 17%, 13%, and 11%, respectively. This was correlated with the formation of char which acted as a barrier for heat and mass transfer between the flame zone and the underlying sample.[51] PBT ignited after 53 s of exposure to 35 kW/m^2 external heat flux, while the reinforced PBT composites had earlier ignition at 42–50 s. The work of Dittrich on the carbon nanomaterials-reinforced PP nanocomposites suggested that the TTI value is dependent on the thermal conductivity and heat absorption of the materials.[43] The shorter TTI was attributed to the greater in-depth heat absorption of filled-PP nanocomposites than the neat PP. Time to PHRR also showed decrement after the inclusion of fillers. Lower TTI values with the addition of 1 wt% fillers were reported on PBT nanocomposites filled with functionalized CNTs[52] and Sb$_2$O$_3$.[53]

With respect to material safety, PBT/SWN 1.0 nanocomposite with an FPI value of 0.1011, ranked the highest among the samples, due to its higher TTI. The FPI values for neat PBT and PBT/NW composites are very close, which are 0.0927 and 0.0929 m^2 s/kW, respectively. However, PBT/GO nanocomposites exhibited deteriorated material safety when compared to neat PBT. This is attributed to its lowest TTI value, which evinced the earliest ignition of the sample. Moreover, Table 3 showed that the addition of fillers in PBT matrix reduced the FIGRA values,

mainly by reducing the PHRR values. PBT/NW composites exhibited the highest efficiency in reducing the FIGRA, followed by PBT/SWN nanocomposite and PBT/GO nanocomposite. The PSPR, PCO$_2$P, and PCOP values of PBT were reduced after the incorporation of fillers. The results indicate that the reinforced PBT composites had lower fire hazards as the release of smoke and toxic gases were suppressed throughout the combustion process.

4 | CONCLUSIONS

PBT composites filled with NW, SWN, and GO were successfully prepared to improve the mechanical, thermal, tribological, and flammability properties. The result showed that PBT/SWN 1.0 nanocomposite had the most balanced Young's modulus and impact strength properties. It exhibited the maximum improvement of 6% and 9% in tensile strength and Young's modulus, which was followed by PBT/NW 1.0 composite (+1.3% and +7%) and PBT/GO 1.0 nanocomposite (−2% and +4%). SWN is a better reinforcing filler as compared to NW and GO due to its better interfacial interactions with the PBT matrix and its uniform dispersion. The addition of any of the fillers induced a decrement in elongation at break and impact strength. Material that has better mechanical properties worn off lesser in the sliding test. PBT/SWN nanocomposite performed the best for wear resistance properties with 73% reduction in W_s. Interestingly, the multilayered structure of GO allowed an excellent lubricating effect and contributed to the lowest μ of PBT/GO 1.0 nanocomposite with 26% reduction. Due to its high angularity and small back transfer film formed, PBT/NW 1.0 composite lowered μ by only 4%.

Furthermore, all the fillers marginally influenced the T_m, T_c, and X_c of PBT. The PBT/NW, PBT/SWN, and PBT/GO composites had 4°C, 13.8°C and 9.5°C higher T_{max}, achieving 399.5°C, 409°C, and 404.7°C, respectively. NW and SWN slightly increased the residue weight, but the self-propagating reduction of GO reduced the residue weight. PBT/NW composite performed the best flame retardancy with respect to the PHRR, smoke and carbon dioxide production rate. It is found that the physical

morphology and size of the fillers played an important role in determining the functional properties of PBT composites. The SWN was found to be a promising reinforcing filler for better mechanical properties, wear resistance and thermal stability performances, while GO exhibited an excellent lubricating effect. This study suggests that PBT nanocomposites are suitable to be applied as lightweight structural components for automobiles. It is proposed that future work on the synergic effects of SWN and GO in PBT matrix may be carried out for automotive applications such as in the use of bearing and bushing applications. Similar PBT-based composites fabricated using different melt compounding techniques or processing parameters can be done to improve the filler dispersion. Considering the low ductility and impact strength, the introduction of a suitable impact modifier or surface modifying agent into PBT-based composites is worth investigating.

AUTHOR CONTRIBUTIONS

Jia Xin Chan: Conceptualization (lead); formal analysis (lead); investigation (lead); validation (equal); writing – original draft (lead). **Joon Fatt Wong:** Investigation (supporting); validation (equal); writing – review and editing (equal). **Azman Hassan:** Conceptualization (lead); supervision (lead); validation (equal); writing – review and editing (equal). **Norhayani Othman:** Conceptualization (lead); supervision (lead); validation (equal); writing – review and editing (equal). **Jeefferie Abd Razak:** Methodology (equal); resources (equal); supervision (supporting); writing – review and editing (equal). **Umar Nirmal:** Supervision (supporting); validation (equal); visualization (lead); writing – review and editing (equal). **Shahrir Hashim:** Funding acquisition (lead); project administration (lead); writing – review and editing (equal). **Yern Chee Ching:** Methodology (equal); resources (equal); writing – review and editing (equal). **Muhamad Zaini Yunos:** Methodology (equal); resources (equal); writing – review and editing (equal). **Ridwan Yahaya:** Investigation (supporting); resources (equal); writing – review and editing (equal). **T.M. Sampath U. Gunathilake:** Methodology (equal); resources (equal); writing – review and editing (equal).

CONFLICT OF INTEREST
The authors declare that they have no known competing financial interests or personal relationships that could have appeared to influence the work reported in this paper.

DATA AVAILABILITY STATEMENT
The data that support the findings of this study are available in the supplementary material of this article.

ORCID
Azman Hassan https://orcid.org/0000-0002-4247-9158

REFERENCES
[1] I. C. Kim, K. H. Kwon, W. N. Kim, *J. Appl. Polym. Sci.* **2019**, *136*, 1.
[2] M. Li, Y. G. Jeong, *J. Appl. Polym. Sci.* **2012**, *125*, 2658.
[3] G. S. Deshmukh, D. R. Peshwe, S. U. Pathak, J. D. Ekhe, *Trans. Indian Inst. Metals* **2011**, *64*, 127.
[4] K. A. Deshmukh, S. Chopra, P. Khajanji, A. Deshmukh, D. R. Peshwe, *Polym. Bull.* **2022**, *79*, 381.
[5] B. Ucpinar Durmaz, M. G. Atılgan, A. Aytac, *Iran. Polym. J.* **2022**, *31*, 991.
[6] Z. Li, W. Li, L. Liao, J. Li, T. Wu, L. Ran, T. Zhao, B. Chen, *J. Appl. Polym. Sci.* **2020**, *137*, 1.
[7] P. Russo, A. Costantini, G. Luciani, F. Tescione, M. Lavorgna, F. Branda, B. Silvestri, *J. Appl. Polym. Sci.* **2018**, *135*, 1.
[8] Z. Gao, Q. Dong, M. Shang, B. Shentu, C. Wu, *J. Appl. Polym. Sci.* **2022**, *139*, 51733.
[9] L. Lapčík, D. Maňas, B. Lapčíková, M. Vašina, M. Staněk, K. Čépe, J. Vlček, K. E. Waters, R. W. Greenwood, N. A. Rowson, *Compos. B: Eng.* **2018**, *141*, 92.
[10] Q. Ding, Z. Zhang, X. Dai, M. Li, K. Mai, *Polym. Compos.* **2019**, *40*, E638.
[11] L. Teng Saw, F. Zainuddin, C. Xuan Viet, D. N. Uy Lan, *IOP Conf. Ser. Mater. Sci. Eng.* **2020**, *864*, 012114.
[12] S. Sharma, J. Bijwe, S. Panier, M. Sharma, *Wear* **2015**, *332–333*, 863.
[13] B. P. Chang, A. K. Mohanty, M. Misra, *J. Appl. Polym. Sci.* **2019**, *136*, 1.
[14] G. S. Deshmukh, D. R. Peshwe, S. U. Pathak, J. D. Ekhe, *Thermochim. Acta* **2014**, *581*, 41.
[15] J. X. Chan, J. F. Wong, A. Hassan, Z. Mohamad, N. Othman, *Polym. Compos.* **2020**, *41*, 395.
[16] J. F. Wong, J. X. Chan, A. B. Hassan, Z. B. Mohamad, N. B. Othman, *J. Mater. Sci.* **2021**, *56*, 8911.
[17] S. N. Danilova, S. B. Yarusova, Y. N. Kulchin, I. G. Zhevtun, I. Y. Buravlev, A. A. Okhlopkova, P. S. Gordienko, E. P. Subbotin, *Polymers (Basel).* **2021**, *13*, 570.
[18] A. S. Luyt, M. D. Dramićanin, Ž. Antić, V. Djoković, *Polym. Test.* **2009**, *28*, 348.
[19] J. F. Wong, J. X. Chan, A. Hassan, Z. Mohamad, S. Hashim, J. Abd Razak, Y. C. Ching, Z. Yunos, R. Yahaya, *Polym. Compos.* **2022**, *43*, 7845.
[20] J. X. Chan, J. F. Wong, A. Hassan, N. K. Shrivastava, Z. Mohamad, N. Othman, *Ceram. Int.* **2020**, *46*, 22624.
[21] J. A. Puértolas, M. Castro, J. A. Morris, R. Ríos, A. Ansón-Casaos, *Carbon N. Y.* **2019**, *141*, 107.
[22] S. H. Yetgin, *Bull. Mater. Sci.* **2020**, *43*, 89.
[23] J. Bian, H. L. Lin, F. X. He, L. Wang, X. W. Wei, I. T. Chang, E. Sancaktar, *Eur. Polym. J.* **2013**, *49*, 1406.
[24] P. Qian, Y. Zhang, H. Mao, H. Wang, H. Shi, *SN Appl. Sci.* **2019**, *1*, 443.
[25] J. X. Chan, J. F. Wong, A. Hassan, N. Othman, J. A. Razak, U. Nirmal, S. Hashim, Y. C. Ching, M. Z. Yunos, R. Yahaya, T. M. S. U. Gunathilake, *Polymer (Guildf).* **2022**, *256*, 125259.

[26] G. Broza, M. Kwiatkowska, Z. Rosłaniec, K. Schulte, *Polymer (Guildf).* **2005**, *46*, 5860.

[27] S. S. Chee, M. Jawaid, O. Y. Alothman, R. Yahaya, *RSC Adv.* **2020**, *10*, 21686.

[28] P. Yu, R. J. Kirkpatrick, B. Poe, P. F. McMillan, X. Cong, *J. Am. Ceram. Soc.* **2004**, *82*, 742.

[29] P. Marciniak, B. Sztorch, A. Martyła, A. Czapik, M. Stodolny, R. E. Przekop, *Ceramics* **2021**, *4*, 278.

[30] M. Bouatrous, F. Bouzerara, A. K. Bhakta, F. Delobel, J. Delhalle, Z. Mekhalif, *Ceram. Int.* **2020**, *46*, 12618.

[31] Z. G. Mohammadsalih, B. J. Inkson, B. Chen, *Polym. Compos.* **2021**, *42*, 320.

[32] B. Zhao, T. Bai, *Carbon N. Y.* **2019**, *144*, 481.

[33] H. Li, Z. Wei, *Polymers (Basel)* **2021**, *13*, 2431.

[34] R. S. Tarade, P. A. Mahanwar, *J. Mater. Environ. Sci* **2019**, *10*, 357.

[35] Y. S. Yun, Y. H. Bae, D. H. Kim, J. Y. Lee, I. Chin, H. Jin, *Carbon N. Y.* **2011**, *49*, 3553.

[36] Y. Chen, Y. Qi, Z. Tai, X. Yan, F. Zhu, Q. Xue, *Eur. Polym. J.* **2012**, *48*, 1026.

[37] R. S. Tarade, P. A. Mahanwar, *J. Vinyl Addit. Technol.* **2020**, *26*, 481.

[38] A. Nourbakhsh, A. Karegarfard, A. Ashori, A. Nourbakhsh, *J. Thermoplast. Compos. Mater.* **2010**, *23*, 169.

[39] S. Y. Fu, X. Q. Feng, B. Lauke, Y. W. Mai, *Compos. B: Eng.* **2008**, *39*, 933.

[40] B. H. Soudmand, K. Shelesh-Nezhad, Y. Salimi, *J. Appl. Polym. Sci.* **2020**, *137*, 49260.

[41] A. Chatterjee, P. S. Khobragade, S. Mishra, *J. Appl. Polym. Sci.* **2015**, *132*, 42811.

[42] G. Bheemaneni, S. Saravana, R. Kandaswamy, *Mater. Today Proc.* **1807**, *2018*, 5.

[43] B. Dittrich, K. A. Wartig, D. Hofmann, R. Mülhaupt, B. Schartel, *Polym. Degrad. Stab.* **2013**, *98*, 1495.

[44] F. Kim, J. Luo, R. Cruz-Silva, L. J. Cote, K. Sohn, J. Huang, *Adv. Funct. Mater.* **2010**, *20*, 2867.

[45] Y. He, Q. Chen, H. Liu, L. Zhang, D. Wu, C. Lu, W. OuYang, D. Jiang, M. Wu, J. Zhang, Y. Li, J. Fan, C. Liu, Z. Guo, *Macromol. Mater. Eng.* **2019**, *304*, 1900166.

[46] B. Chen, X. Li, Y. Jia, L. Xu, H. Liang, X. Li, J. Yang, C. Li, F. Yan, *Compos. Part A: Appl. Sci. Manuf.* **2018**, *115*, 157.

[47] I. K. Aliyu, A. S. Mohammed, A. Al-Qutub, *Polym. Compos.* **2019**, *40*, E1301.

[48] J. Tong, Y. Ma, R. D. Arnell, L. Ren, *Compos. Part A: Appl. Sci. Manuf.* **2006**, *37*, 38.

[49] K. Friedrich, *Adv. Ind. Eng. Polym. Res.* **2018**, *1*, 3.

[50] C. Liu, Y. Dong, Y. Lin, H. Yan, W. Zhang, Y. Bao, J. Ma, *Compos. B: Eng.* **2019**, *165*, 491.

[51] B. Schartel, M. Bartholmai, U. Knoll, *Polym. Adv. Technol.* **2006**, *17*, 772.

[52] S.-E. Zhu, L.-L. Wang, H. Chen, W. Yang, A. Yuen, T. Chen, C. Luo, W.-M. Bi, E.-Z. Hu, J. Zhang, J.-Y. Si, H.-D. Lu, K.-H. Hu, Q. Chan, G. Yeoh, *Nanomaterials* **2018**, *8*, 70.

[53] L. Niu, J. Xu, W. Yang, J. Ma, J. Zhao, C. Kang, J. Su, *Materials (Basel).* **2018**, *11*, 1060.

SUPPORTING INFORMATION

Additional supporting information can be found online in the Supporting Information section at the end of this article.